

# Superposition Model for Dielectric Charging of RF MEMS Capacitive Switches Under Bipolar Control-Voltage Waveforms

Zhen Peng, *Student Member, IEEE*, Xiaobin Yuan, *Member, IEEE*, James C. M. Hwang, *Fellow, IEEE*, David I. Forehand, *Member, IEEE*, and Charles L. Goldsmith, *Senior Member, IEEE*

**Abstract**—Bipolar control-voltage waveforms, under which the control voltage alternates between positive and negative after each cycle, have been proposed to mitigate dielectric charging in electrostatically actuated RF microelectromechanical system capacitive switches. In this study, dielectric charging under bipolar waveforms is modeled and characterized quantitatively. In general, the experimental results agree with predictions based on the superposition of unipolar charging models that are extracted under positive and negative voltages, respectively. The basic assumptions for such a superposition model are examined in detail and validated experimentally. The current analysis indicates that, while bipolar waveforms can reduce charging, it is difficult to fine tune the waveforms to completely eliminate charging.

**Index Terms**—Charge injection, dielectric films, dielectric materials, microelectromechanical devices, switches.

## I. INTRODUCTION

CURRENTLY, the life time of electrostatically actuated RF microelectromechanical system (MEMS) capacitive switches is primarily limited by dielectric charging, which can cause actuation-voltage shift or, ultimately, stiction [1]–[25]. Experimentally, the dielectric charging phenomenon has been investigated by monitoring shifts in RF transmission characteristics [24], electrostatic and adhesion forces [14], capacitance–voltage characteristics [2]–[6], [8]–[11], [16], and current–voltage characteristics [7], [17], [18], [20], [25] with an increasing level of physical understanding. For example, charge transport was shown to be through the Frenkel–Poole mechanism [11]. Material quality was found to have strong effects on depolarization current [19] and discharging current [20]. Theoretically, a qualitative charging model was proposed

[4] and various charge distributions were assumed [6]. A quantitative charging model was developed and validated [21] for charging from the bottom electrode [22] under unipolar control-voltage waveforms of different frequencies, voltages, and duty factors, as well as under different ambient temperatures.

In this paper, to mitigate the charging problem, bipolar control-voltage waveforms [e.g., No. 2–No. 4 in Table II and Fig. 2(b)], as opposed to unipolar control-voltage waveforms [e.g., No. 1 and 5 in Table II and Fig. 2(b)], have been proposed [2]. Under a bipolar waveform, the control voltage alternates between positive and negative after each switching cycle. If a positive voltage is used to actuate a switch in one cycle, a negative voltage will be used to actuate the switch in the following cycle and vice versa. Since positive and negative voltages are equally effective in actuating the switch, the switch will function as if it is under a unipolar waveform. However, incremental charging during each cycle will alternate between positive and negative so that the cumulative effect will supposedly be minimized. Such a cancellation effect was, for the first time, modeled and characterized in [25]. The model is based on the superposition of unipolar charging models that are extracted under positive and negative voltages, respectively [18]. In spite of the simplification, the superposition model predictions are in general agreement with bipolar charging experiments under different switching frequencies, voltages, and duty factors [25]. This paper expands on [25] by examining the superposition assumptions in detail and by justifying the assumptions through additional experimental data.

Fig. 1 illustrates the construction of the current RF MEMS capacitive switches. The dielectric is sputtered SiO<sub>2</sub> with a thickness of 0.3 μm and a dielectric constant of 5.5. The top electrode is a moveable 0.3-μm-thick Al membrane that is permanently grounded. The bottom Cr/Au electrode serves as the center conductor of a 50-Ω coplanar waveguide for the RF signal. Without any electrostatic force, the Al membrane is normally suspended in air 2.2 μm above the dielectric. A control voltage, either positive or negative, is applied to the bottom electrode, which pulls the membrane in contact with the dielectric, thereby forming a 120 μm × 80 μm capacitor to shunt the RF signal to ground. At 35 GHz, this results in >15-dB isolation at the on state (membrane down) and <0.1-dB insertion loss at the off state (membrane up). The actuation or pull-down voltage  $V$  is typically ±25 V, while the release voltage is typically ±10 V. The switching time is less than 10 μs.

Manuscript received May 8, 2007; revised August 1, 2007. This work was supported in part by the U.S. Air Force Research Laboratory under Contract F33615-03-C-7003, funded by the U.S. Defense Advanced Research Projects Agency under the Harsh Environment, Robust Micromechanical Technology (HERMIT) Program.

Z. Peng and J. C. M. Hwang are with the Department of Electrical and Computer Engineering, Lehigh University, Bethlehem, PA 18015 USA (e-mail: zhp205@lehigh.edu).

X. Yuan is with the Semiconductor Research and Development Center, IBM Corporation, Hopewell Junction, NY 12533 USA.

D. I. Forehand and C. L. Goldsmith are with the MEMtronics Corporation, Plano, TX 75075 USA.

Color versions of one or more of the figures in this paper are available online at <http://ieeexplore.ieee.org>.

Digital Object Identifier 10.1109/TMTT.2007.909475

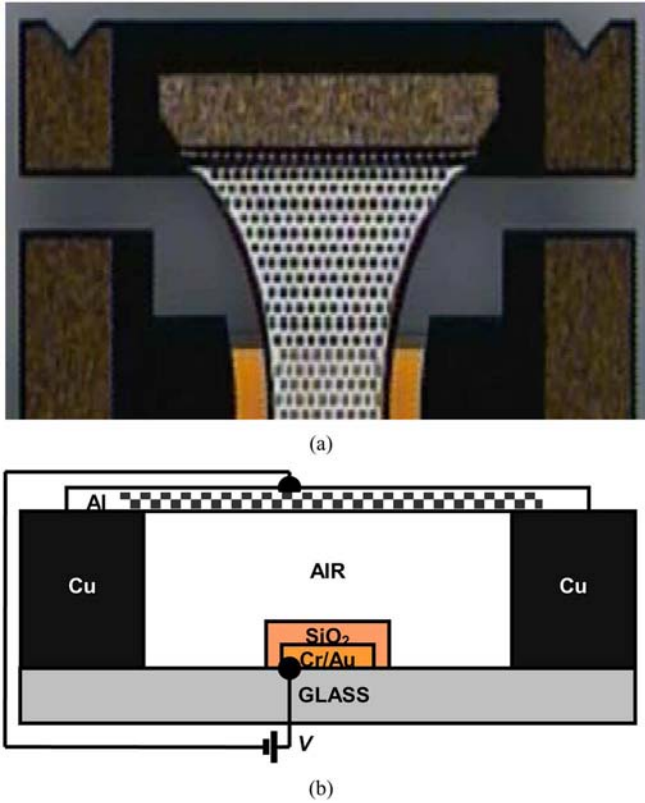


Fig. 1. (a) Top and (b) cross-sectional views of a state-of-the-art RF MEMS capacitive switch. In (a), only the top half of the switch is shown, the bottom half being a mirror image of the top half. In (b), the vertical scale is expanded by approximately 60× for clarity.

## II. MODEL CONSTRUCTION

Although the actuation voltage is only  $\pm 25$  V, control voltages up to  $\pm 40$  V are used to accelerate charging during accelerated life tests of the switch. These control voltages are high enough to cause charge injection from the bottom electrode into the dielectric, yet low enough to avoid charge injection from the top electrode into the dielectric [22]. In fact, for the current switches, the top-charging threshold is approximately  $\pm 50$  V, while the bottom-charging threshold is approximately  $\pm 10$  V. Under a positive control voltage, positive charge is injected from the bottom electrode into the dielectric (physically, electrons migrate from the dielectric to the bottom electrode, leaving positive charge behind in the dielectric), which can help pull down the membrane, thereby reducing the control voltage required for actuation from, for example, 25 to 24 V. On the other hand, under a negative control voltage, negative charge is injected from the bottom electrode into the dielectric, which can gradually increase the actuation voltage from, for example,  $-25$  to  $-24$  V. Therefore, regardless of the sign of the control voltage, while top charging always increases the magnitude of the actuation voltage, bottom charging always decreases the magnitude of the actuation voltage.

According to [18], charging-induced actuation-voltage shift can be expressed as follows:

$$\Delta V = -hQ/\epsilon \quad (1)$$

where the electrostatic effect of the distributed charge throughout the dielectric is approximated by a sheet charge of density  $Q$  located at height  $h$  above the bottom electrode, and  $\epsilon$  is the dielectric constant. Since the distribution of the charge in the dielectric cannot be directly measured,  $h$  remains a fitting parameter. A single  $h$  value of  $0.12 \mu\text{m}$  was found to give the best fit between model predictions and measured actuation-voltage shifts for the current switch under all control-voltage waveforms.

Following [18], unipolar charging under either positive or negative voltage was separately characterized on  $500 \mu\text{m} \times 500 \mu\text{m}$  fixed Cr–SiO–Al capacitors that were fabricated together with the MEMS switches on the same wafer. Capacitors instead of switches are used because the former have larger contact area and proportionally larger charging/discharging currents, which are still in the femto-ampere range. The capacitors also have more consistent contact between the top electrode and dielectric, while the top contact of the switches may vary according to surface conditions. Obviously, the charging model extracted from the capacitors needs to be validated on switches and is only applicable to bottom charging (as opposed to top charging).

The transient behaviors of charging and discharging currents measured on the fixed capacitors were found [18] to be basically exponential, but never truly saturated even after many hours. Therefore, the accumulated charge in the dielectric is fitted with a series of exponential terms of different time constants

$$Q_{\pm} = \sum_{J=1,2,\dots} Q_{0J\pm} (1 - e^{-\frac{t_{\text{ON}\pm}}{\tau_{CJ\pm}}}) e^{-\frac{t_{\text{OFF}\pm}}{\tau_{DJ\pm}}} \quad (2)$$

where the subscripts “+” and “−” denote charging under positive and negative voltages, respectively,  $Q_0$  is the steady-state charge density (usually,  $Q_+ > 0$  and  $Q_- < 0$ ),  $t_{\text{ON}}$  and  $t_{\text{OFF}}$  are on and off times of the switching cycle, and  $\tau_C$  and  $\tau_D$  are charging and discharging time constants. For rapid convergence during model simulation, simple exponential terms are used instead of the stretched exponential function [10]. In addition, the summation is usually truncated at  $J = 2$ . Higher order terms can be used to increase precision at the expense of difficult extraction.

The steady-state charge density, in turn, was found [18] to increase exponentially with voltage so that

$$Q_{0J\pm} = Q_{00J\pm} e^{\frac{V_{\pm}}{V_0}} \quad (3)$$

where  $Q_{00}$  is a pre-exponential factor and  $V_0$  is a voltage scaling factor. Table I lists the extracted values of  $Q_{00}$ ,  $V_0$ ,  $\tau_C$ , and  $\tau_D$  of the current switch. Notice that, except for the sign of  $Q_{00}$ , the values are very similar under positive and negative voltages. This implies that a symmetrical bipolar waveform should indeed minimize charging.

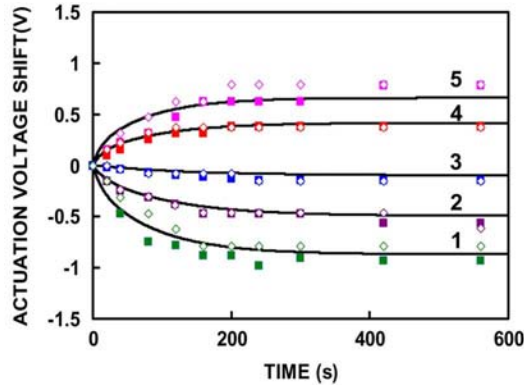
Table II lists the various control-voltage waveforms that are illustrated in Fig. 2(b). For example, at a switching frequency of 10 kHz, the period of a bipolar switching cycle  $\Delta t$  includes one positive switching cycle and one negative switching cycle so that  $\Delta t = t_{\text{ON}+} + t_{\text{OFF}+} + t_{\text{ON}-} + t_{\text{OFF}-} = 100 \mu\text{s}$ .

TABLE I  
 EXTRACTED MODEL PARAMETERS

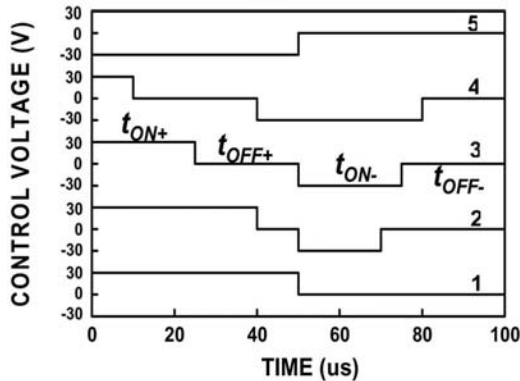
| Positive Voltage |                        |              |                 |                 |
|------------------|------------------------|--------------|-----------------|-----------------|
| $J$              | $Q_{00+}$ ( $q/cm^2$ ) | $V_{0+}$ (V) | $\tau_{C+}$ (s) | $\tau_{D+}$ (s) |
| 1                | $5 \times 10^9$        | 12           | 10              | 15              |
| 2                | $9 \times 10^9$        | 10           | 65              | 130             |
| Negative Voltage |                        |              |                 |                 |
| $J$              | $Q_{00-}$ ( $q/cm^2$ ) | $V_{0-}$ (V) | $\tau_{C-}$ (s) | $\tau_{D-}$ (s) |
| 1                | $-2.5 \times 10^9$     | 10           | 8               | 13              |
| 2                | $-7.5 \times 10^9$     | 10           | 60              | 114             |

 TABLE II  
 CONTROL-VOLTAGE WAVEFORMS

| No. | $V_+$ (V) | $V_-$ (V) | $t_{ON+}$ ( $\mu s$ ) | $t_{OFF+}$ ( $\mu s$ ) | $t_{ON-}$ ( $\mu s$ ) | $t_{OFF-}$ ( $\mu s$ ) |
|-----|-----------|-----------|-----------------------|------------------------|-----------------------|------------------------|
| 1   | 30        | --        | 50                    | 50                     | --                    | --                     |
| 2   | 30        | -30       | 40                    | 10                     | 20                    | 30                     |
| 3   |           |           | 25                    | 25                     | 25                    | 25                     |
| 4   |           |           | 10                    | 30                     | 40                    | 20                     |
| 5   | --        | -30       | --                    | --                     | 50                    | 50                     |
| 6   | 35        | -35       | 10                    | 30                     | 40                    | 20                     |
| 7   | 40        | -40       |                       |                        |                       |                        |
| 8   | 35        | -30       |                       |                        |                       |                        |
| 9   | 30        | -35       |                       |                        |                       |                        |



(a)



(b)

Fig. 2. (a) Measured (symbol) versus modeled (curve) actuation-voltage shifts under control-voltage waveforms No. 1–No. 5 (Table II) and illustrated in (b). The switching frequency is (■) 10 Hz and (◇) 10 kHz in (a), but 10 kHz only in (b).

After several bipolar switching cycles, due to the subtle difference between positive and negative charging behaviors, a small

amount of charge  $Q(t)$  may accumulate in the dielectric. Assuming  $Q(t) > 0$ , it can be fitted to (2) as follows:

$$Q(t) = Q_{0+}(1 - e^{-\frac{t'}{\tau_{C+}}}) \quad (4)$$

where  $t'$  is the equivalent time it takes to accumulate  $Q(t)$  under a constant positive voltage. In other words, as far as charging is concerned, dc stress for  $t'$  is equivalent to ac stress for  $t$ . Notice that the summation over the subscript  $J$  is omitted for clarity.

During the next switching cycle,

$$\begin{aligned} Q(t + t_{ON+}) &= Q_{0+} \left( 1 - e^{-\frac{t' + t_{ON+}}{\tau_{C+}}} \right) \\ &= Q_{0+} \left[ \left( 1 - e^{-\frac{t'}{\tau_{C+}}} \right) e^{-\frac{t_{ON+}}{\tau_{C+}}} + \left( 1 - e^{-\frac{t_{ON+}}{\tau_{C+}}} \right) \right] \\ &= Q(t) e^{-\frac{t_{ON+}}{\tau_{C+}}} + Q_{0+} \left( 1 - e^{-\frac{t_{ON+}}{\tau_{C+}}} \right) \end{aligned} \quad (5)$$

$$\begin{aligned} Q(t + t_{ON+} + t_{OFF+}) &= Q(t + t_{ON+}) e^{-\frac{t_{OFF+}}{\tau_{D+}}} \end{aligned} \quad (6)$$

and

$$\begin{aligned} Q(t + t_{ON+} + t_{OFF+} + t_{ON-}) &= Q(t + t_{ON+} + t_{OFF+}) e^{-\frac{t_{ON-}}{\tau_{D+}}} + Q_{0-} \left( 1 - e^{-\frac{t_{ON-}}{\tau_{C-}}} \right). \end{aligned} \quad (7)$$

In (7), we assume *discharging of the positive charge under a negative voltage is the same as that without any applied voltage, while negative charging is unaffected by any accumulated positive charge*. These assumptions justify the use of the superposition principle. They will be examined in detail in Section III. Finally,

$$Q(t + \Delta t) = Q(t + t_{ON+} + t_{OFF+} + t_{ON-}) e^{-\frac{t_{OFF-}}{\tau_{D-}}}. \quad (8)$$

Thus, starting with  $Q(0) = 0$ , (5)–(8) can be iterated  $n$  times to determine  $Q(n\Delta t)$ .

If  $Q(t) < 0$ , then it is more convenient to start with negative charging during the second half of the bipolar switching cycle so that (5)–(8) can be duplicated, except for sign change. Thus,

$$\begin{aligned} Q(t + t_{ON-}) &= Q(t) e^{-\frac{t_{ON-}}{\tau_{C-}}} + Q_{0-} \left( 1 - e^{-\frac{t_{ON-}}{\tau_{C-}}} \right) \end{aligned} \quad (9)$$

$$\begin{aligned} Q(t + t_{ON-} + t_{OFF-}) &= Q(t + t_{ON-}) e^{-\frac{t_{OFF-}}{\tau_{D-}}} \end{aligned} \quad (10)$$

$$\begin{aligned} Q(t + t_{ON-} + t_{OFF-} + t_{ON+}) &= Q(t + t_{ON-} + t_{OFF-}) e^{-\frac{t_{ON+}}{\tau_{D-}}} \\ &\quad + Q_{0+} \left( 1 - e^{-\frac{t_{ON+}}{\tau_{C+}}} \right) \end{aligned} \quad (11)$$

$$\begin{aligned} Q(t + \Delta t) &= Q(t + t_{ON-} + t_{OFF-} + t_{ON+}) e^{-\frac{t_{OFF+}}{\tau_{D+}}}. \end{aligned} \quad (12)$$

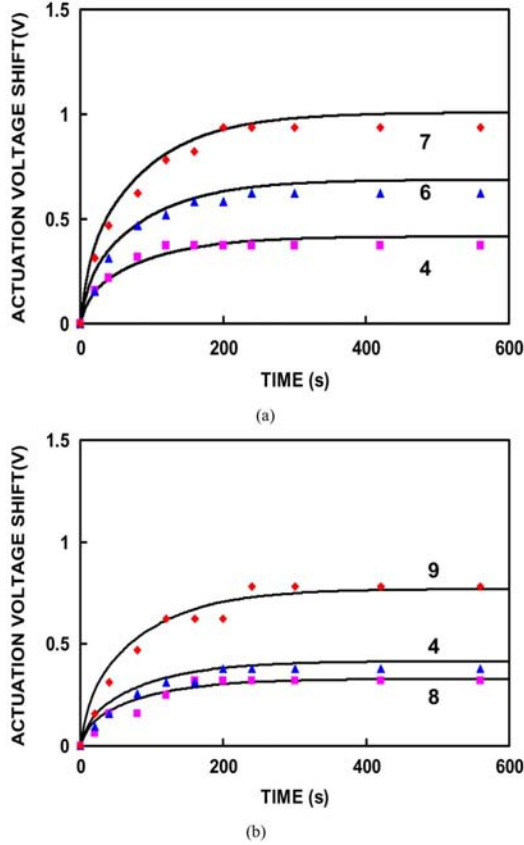


Fig. 3. Measured (symbol) versus modeled (curve) actuation-voltage shifts under control-voltage waveforms: (a) 4, 6, and 7 and (b) 4, 8, and 9, as listed in Table II. The switching frequency is 10 kHz.

In (11), we assume *discharging of the negative charge under a positive voltage is the same as that without any applied voltage, while positive charging is unaffected by any accumulated negative charge*. These assumptions will also be examined in detail in Section III.

Once  $Q$  is found through iterations of (5)–(8) or (9)–(12), (1) can be used to predict the actuation-voltage shift of switch. The predicted actuation-voltage shift is then compared with experimental data, as discussed in the following.

### III. RESULTS AND DISCUSSION

Using a previously developed [18] test setup and procedure, actuation-voltage shifts under control-voltage waveforms of different frequencies, voltages, and duty factors were measured on real switches and compared with model predictions based on fixed capacitors, as shown in Figs. 2 and 3. As can be seen in these figures, general agreement was found in all cases examined. Similar to unipolar charging [18], bipolar charging, although of smaller magnitude, increases with stress time and voltage, but is independent of switching frequency as long as the switching cycle is much shorter than charging/discharging time constants.

As mentioned earlier, due to the subtle difference between positive and negative charging, a small amount of charge gradually accumulates even under a symmetrical bipolar waveform

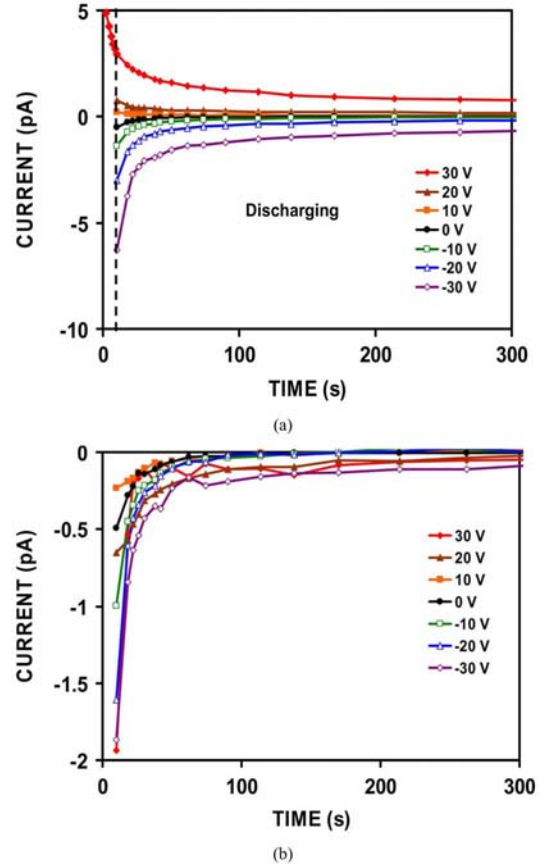


Fig. 4. (a) Measured discharging currents under different discharging voltages, after a capacitor is charged at 30 V for 10 s (left of the dashed line). (b) Same measured discharging currents after subtracting the charging currents by the discharging voltages themselves.

[No. 3 in Table II or Fig. 2(b)]. Thus, it is tempting to fine tune the waveform in order to exactly balance out positive and negative charging within each switching cycle. This implies that

$$Q_{0+} \left( 1 - e^{-\frac{t_{ON+}}{\tau_{C+}}} \right) e^{-\frac{t_{OFF++} + t_{ON-}}{\tau_{D+}}} = Q_{0-} \left( 1 - e^{-\frac{t_{ON-}}{\tau_{C-}}} \right). \quad (13)$$

Usually, the switching cycle is much shorter than charging/discharging time constants and (13) can be simplified as follows:

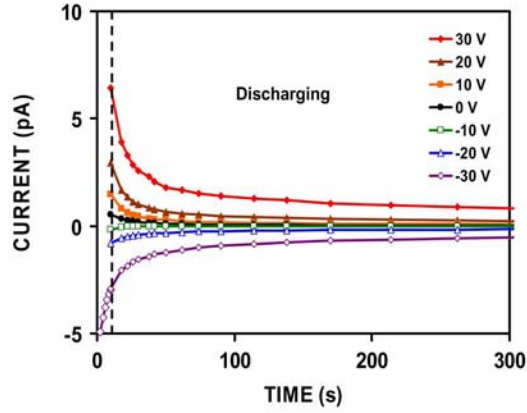
$$Q_{0+} t_{ON+} / \tau_{C+} \cong Q_{0-} t_{ON-} / \tau_{C-} \quad (14)$$

OR

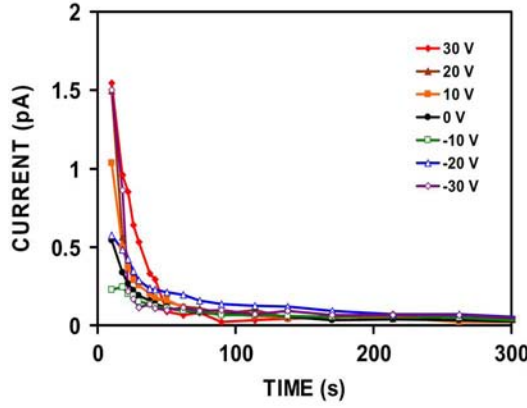
$$t_{ON+} / t_{ON-} \cong Q_{0-} \tau_{C+} / Q_{0+} \tau_{C-}. \quad (15)$$

Therefore, for such a delicate balance within each bipolar switching cycle, the on times of positive and negative voltages need to be fine tuned according to (15). If the application calls for  $t_{ON+} = t_{ON-}$ , then

$$Q_{0+} / Q_{0-} \cong \tau_{C+} / \tau_{C-}. \quad (16)$$



(a)



(b)

Fig. 5. (a) Measured discharging currents under different discharging voltages, after a capacitor is charged at  $-30$  V for 10 s (left of the dashed line). (b) Same measured discharging currents after subtracting the charging currents by the discharging voltages themselves.

From (3),

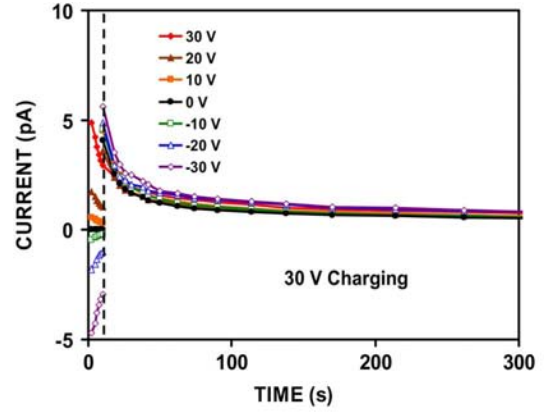
$$Q_{00+} \exp(V_+/V_{0+})/Q_{00-} \exp(V_-/V_{0-}) \cong \tau_{C+}/\tau_{C-}. \quad (17)$$

Since  $Q_{00+} \sim Q_{00-}$  and  $\tau_{C+} \sim \tau_{C-}$ ,

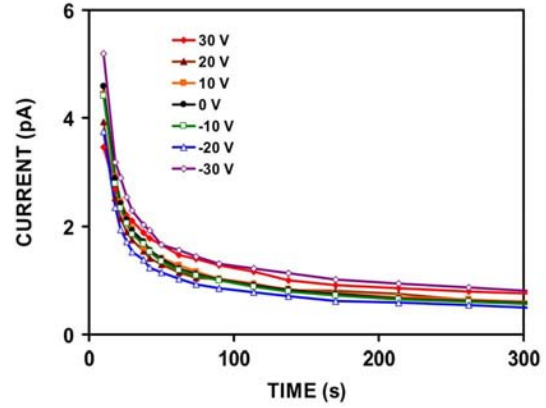
$$V_+/V_- \cong V_{0+}/V_{0-}. \quad (18)$$

However, due to the exponential voltage dependence of (17), (18) is difficult to exactly satisfy, especially if higher order terms are included in the summation over  $J$ .

The current model is based on the superposition principle. The superposition principle applies to the current Cr–SiO<sub>2</sub>–Al capacitors probably because they have similar charging behaviors under both positive and negative voltages without strong interaction between positive charging and negative charging. As mentioned in Section II, we assume *discharging of positive charge under negative voltage is the same as that without any voltage, while negative charging is unaffected by accumulated positive charge*. Conversely, we assume *discharging of negative charge under positive voltage is the same as that without any voltage, while positive charging is unaffected by accumulated*



(a)



(b)

Fig. 6. (a) Measured charging currents at 30 V after a capacitor is charged under different charging voltages for 10 s (left of the dashed line). (b) Same measured charging currents after subtracting the discharging currents by the initial charging voltages.

*negative charge*. These assumptions are examined experimentally as follows.

In [18], charging currents were measured on fixed capacitors under constant control voltages, while discharging currents were measured without any control voltage. To validate the above-mentioned assumptions, charging currents are measured the same as before, but discharging currents are now measured under different control voltages. Fig. 4(a) shows the discharging currents measured on a capacitor that was first charged under 30 V for 10 s, which is of the order of the first-order charging time constant. As is, it appears that the discharging current is strongly dependent on the discharging voltage. However, after the charging current by the discharging voltage itself [calculated according to (2)] is subtracted from the net discharging current, Fig. 4(b) shows that discharging of the original charge accumulated under 30 V is not a strong function of the discharging voltage. Similarly, Fig. 5(b) shows that discharging of the charge accumulated under  $-30$  V is not a strong function of discharging voltage.

Using similar approaches, Fig. 6 confirms that positive charging is not strongly affected by various amounts of accumulated positive or negative charge, while Fig. 7 confirms that negative charging is not strongly affected by various amounts of accumulated negative or positive charge. This is because,

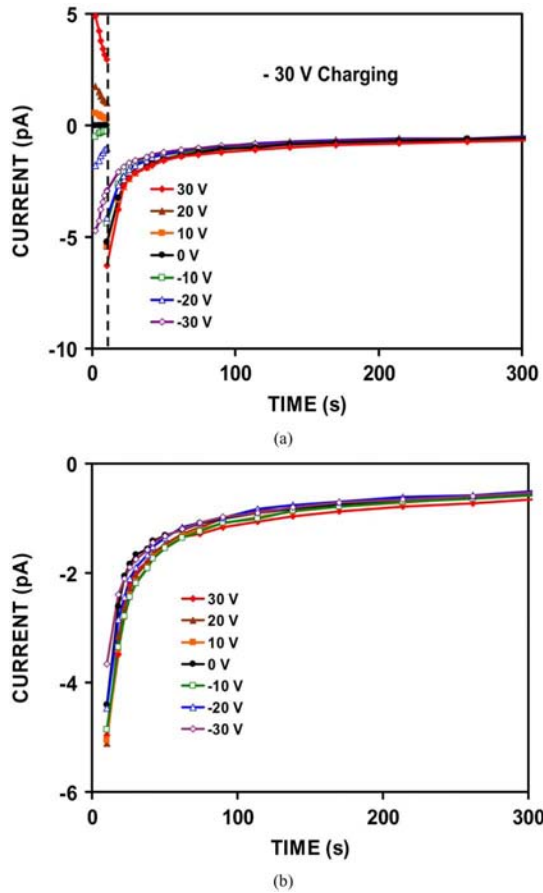


Fig. 7. (a) Measured charging currents at  $-30$  V after a capacitor is charged under different charging voltages for 10 s (left of the dashed line). (b) Same measured charging currents after subtracting for the discharging currents by the initial charging voltages.

although the superposition assumptions are at best approximations, the resulted errors tend to cancel each other. For example, the right side of (7) consists of a positive term and a negative term ( $Q > 0$ , while  $Q_{0-} < 0$ ). Under the superposition assumptions, the absolute magnitudes of both terms would be underestimated, resulting in a net error smaller than the error of either term. Thus, it is not surprising that (7) and (11) can model charging/discharging reasonably well when the control voltage changes from positive to negative or vice versa, as shown in Fig. 8. This is also why (5)–(8) or (9)–(12) can model actuation-voltage shifts under different bipolar waveforms, as shown in Figs. 2 and 3.

Table I shows that the first-order charging/discharging time constants are of the order of 10 s, while the second-order charging/discharging time constants are of the order of  $10^2$  s. In this paper, the charging/discharging model is truncated *after* the second-order terms so that the experimental validation is truncated after  $10^3$  s. For high-cycle life tests [24] that last for many months or  $10^5$  s, it will be necessary to extract higher order model terms with correspondingly longer time constants. However, as mentioned before, higher order terms are increasingly more difficult to extract due to instrument noise and drift.

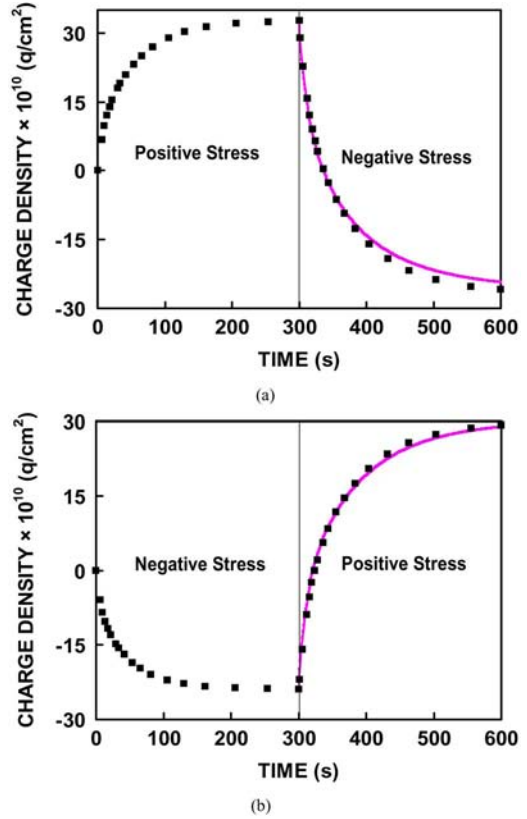


Fig. 8. Measured (symbol) versus modeled (curve) charge after the control voltage changes: (a) from 30 to  $-30$  V or (b) from  $-30$  to 30 V. The measured charge is based on integrating the measured transient current with time. The modeled charge is based on (7) and (11) in (a) and (b), respectively.

Nevertheless, [24] shows that the current model could be used to optimize the design of the switch to allow billions of cycles of operation, and the charging behavior over  $10^5$  s is consistent with the general trends predicted by the current model. This is probably because most of the charging occurs initially before it gradually diminishes.

#### IV. CONCLUSION

In conclusion, bipolar control-voltage waveforms were found to reduce dielectric charging in RF MEMS capacitive switches. A bipolar charging model was developed from the superposition of unipolar charging models. The model agrees well with the experimental results obtained on real switches under bipolar waveforms of different frequencies, voltages, and duty factors. The model also shows that it is difficult to fine tune the waveform to completely eliminate charging.

#### REFERENCES

- [1] C. Goldsmith, J. Ehmke, A. Malczewski, B. Pillans, S. Eshelman, Z. Yao, J. Brank, and M. Eberly, "Lifetime characterization of capacitive RF MEMS switches," in *IEEE MTT-S Int. Microw. Symp. Dig.*, Jun. 2001, pp. 227–230.
- [2] J. R. Reid and R. T. Webster, "Measurements of charging in capacitive microelectromechanical switches," *Electron. Lett.*, vol. 38, no. 24, pp. 1544–1545, Nov. 2002.
- [3] W. M. van Spengen, R. Puers, R. Mertens, and I. De Wolf, "Experimental characterization of stiction due to charging in RF MEMS," in *IEEE Int. Electron Devices Meeting Dig.*, Dec. 2002, pp. 901–904.

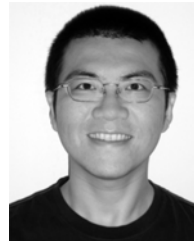
- [4] W. M. van Spengen, R. Puers, R. Mertens, and I. De Wolf, "A comprehensive model to predict the charging and reliability of capacitive RF MEMS switches," *J. Micromech. Microeng.*, vol. 14, pp. 514–521, Jan. 2004.
- [5] X. Yuan, S. V. Cherepko, J. C. M. Hwang, C. L. Goldsmith, C. Nordquist, and C. Dyck, "Initial observation and analysis of dielectric-charging effects on RF MEMS capacitive switches," in *IEEE MTT-S Int. Microw. Symp. Dig.*, Jun. 2004, pp. 1943–1946.
- [6] X. Rottenberg, B. Nauwelaers, W. Raedt, and H. A. C. Tilmans, "Distributed dielectric charging and its impact on RF-MEMS device," in *GAAS 12th Symp. Dig.*, Oct. 2004, pp. 475–478.
- [7] X. Yuan, J. C. M. Hwang, D. Forehand, and C. L. Goldsmith, "Modeling and characterization of dielectric-charging effects in RF MEMS capacitive switches," in *IEEE MTT-S Int. Microw. Symp. Dig.*, Jun. 2005, pp. 753–756.
- [8] S. Melle, D. De Conto, L. Mazenq, D. Dubuc, K. Grenier, L. Bary, O. Vendier, J. L. Cazaux, and R. Plana, "Modeling of the dielectric charging kinetic for capacitive RF-MEMS," in *IEEE MTT-S Int. Microw. Symp. Dig.*, Jun. 2005, pp. 757–760.
- [9] G. J. Papaioannou, M. Exarchos, V. Theonas, G. Wang, and J. Papapolymerou, "On the dielectric polarization effects in capacitive RF-MEMS switches," in *IEEE MTT-S Int. Microw. Symp. Dig.*, Jun. 2005, pp. 761–764.
- [10] G. J. Papaioannou, M. Exarchos, V. Theonas, G. Wang, and J. Papapolymerou, "Temperature study of the dielectric polarization effects of capacitive RF-MEMS switches," *IEEE Trans. Microw. Theory Tech.*, vol. 53, no. 11, pp. 3467–3473, Nov. 2005.
- [11] S. Melle, D. De Conto, D. Dubuc, K. Grenier, O. Vendier, J. L. Muraro, J. L. Cazaux, and R. Plana, "Reliability modeling of capacitive RF MEMS," *IEEE Trans. Microw. Theory Tech.*, vol. 53, no. 11, pp. 3482–3488, Nov. 2005.
- [12] R. W. Herfst, H. G. A. Huizing, P. G. Steeneken, and J. Schmitz, "Characterization of dielectric charging in RF MEMS capacitive switches," in *IEEE Int. Microelectron. Test Structures Conf. Dig.*, Mar. 2006, pp. 133–136.
- [13] J. F. Keko, J. C. Petrosky, J. R. Reid, and K. Yung, "Non-charge related mechanism affecting capacitive MEMS switch lifetime," *IEEE Microw. Wireless Compon. Lett.*, vol. 16, no. 3, pp. 140–142, Mar. 2006.
- [14] S. Patton and J. Zabinski, "Effects of dielectric charging on fundamental forces and reliability in capacitive microelectromechanical systems radio frequency switch contacts," *J. Appl. Phys.*, vol. 99, no. 9, pp. 1700–1710, May 2006.
- [15] X. Yuan, Z. Peng, J. C. M. Hwang, D. Forehand, and C. L. Goldsmith, "Temperature Acceleration of dielectric-charging effects in RF MEMS capacitive switches," in *IEEE MTT-S Int. Microw. Symp. Dig.*, Jun. 2006, pp. 47–50.
- [16] G. J. Papaioannou, M. Exarchos, V. Theonas, J. Psychias, G. Konstantinidis, D. Vasilache, A. Muller, and D. Neculoiu, "Effect of space charge polarization in radio frequency microelectromechanical system capacitive switch dielectric charging," *Appl. Phys. Lett.*, vol. 89, no. 10, pp. 922–924, Sep. 2006.
- [17] D. Molinero, R. Comulada, and L. Castañer, "Dielectric charge measurements in capacitive microelectromechanical switches," *J. Appl. Phys.*, vol. 89, no. 8, pp. 901–903, Sep. 2006.
- [18] X. Yuan, Z. Peng, J. C. M. Hwang, D. Forehand, and C. L. Goldsmith, "A transient SPICE model for dielectric-charging effects in RF MEMS capacitive switches," *IEEE Trans. Electron Devices*, vol. 53, no. 10, pp. 2640–2648, Oct. 2006.
- [19] M. Exarchos, E. Papandreou, P. Pons, M. Lamhamdi, G. J. Papaioannou, and R. Plana, "Charging of radiation induced defects in RF MEMS dielectric films," *Microelectron. Rel.*, vol. 46, no. 9–11, pp. 1695–1699, Sep.–Nov. 2006.
- [20] M. Lamhamdi, J. Guastavino, L. Boudou, Y. Segui, P. Pons, L. Bouscayrol, and R. Plana, "Charging-effects in RF capacitive switches influence of insulating layers composition," *Microelectron. Rel.*, vol. 46, no. 9–11, pp. 1700–1704, Sep.–Nov. 2006.
- [21] X. Yuan, Z. Peng, J. C. M. Hwang, D. Forehand, and C. L. Goldsmith, "Acceleration of dielectric charging in RF MEMS capacitive switches," *IEEE Trans. Device Mater. Rel.*, vol. 6, no. 4, pp. 556–563, Dec. 2006.
- [22] Z. Peng, X. Yuan, J. C. M. Hwang, D. Forehand, and C. L. Goldsmith, "Top versus bottom charging of dielectric in RF MEMS capacitive switches," in *Proc Asia-Pacific Microw. Conf.*, Dec. 2006, pp. 1535–1539.
- [23] S. Melle, C. Bordas, D. Dubuc, K. Grenier, O. Vendier, J. L. Muraro, J. L. Cazaux, and R. Plana, "Investigation of stiction effect in electrostatic actuated RF MEMS devices," in *SiRF Top. Meeting Dig.*, Jan. 2007, pp. 173–176.
- [24] C. L. Goldsmith, D. I. Forehand, Z. Peng, J. C. M. Hwang, and J. L. Ebel, "High-cycle life testing of RF MEMS switches," in *IEEE MTT-S Int. Microw. Symp. Dig.*, Jun. 2007, pp. 1805–1808.
- [25] Z. Peng, X. Yuan, J. C. M. Hwang, D. Forehand, and C. L. Goldsmith, "Dielectric charging of RF MEMS capacitive switches under bipolar control-voltage waveforms," in *IEEE MTT-S Int. Microw. Symp. Dig.*, Jun. 2007, pp. 1817–1820.



**Zhen Peng** (S'06) was born in Shanghai, China, in 1980. He received the B.E. degree in electrical engineering from Shanghai Jiao Tong University, Shanghai, China, in 2003, and is currently working toward the Ph.D. degree in electrical and computer engineering at Lehigh University, Bethlehem, PA.

From 2003 to 2005, he was an Integrated Circuit (IC) Design Engineer with the Ricoh Electronics Company, Shanghai, China, where he focused on low-voltage dc-dc converter circuit design and reliability test. He is currently involved in the research

and development of RF MEMS capacitive switches with a focus on modeling and characterization of charging of different dielectric materials under different electrical stresses.



**Xiaobin Yuan** (S'01–M'06) was born in Beijing, China, in 1978. He received the B.E. degree in electronic engineering from Tsinghua University, Beijing, China, in 2001, and the Ph.D. degree in electrical engineering from Lehigh University, Bethlehem, PA, in 2006.

He is currently with the Semiconductor Research and Development Center, IBM Corporation, Hopewell Junction, NY. His research interests include characterization and compact modeling of deep-submicrometer CMOS, RF/microwave devices,

and reliability modeling of RF MEMS.

Dr. Yuan is a member of the IEEE Electron Devices Society and the IEEE Microwave Theory and Techniques Society (IEEE MTT-S).



**James C. M. Hwang** (M'81–SM'82–F'94) received the B.S. degree in physics from National Taiwan University, Taipei, Taiwan, R.O.C., in 1970, and the M.S. and Ph.D. degrees in material science and engineering from Cornell University, Ithaca, NY, in 1973 and 1976, respectively.

Following 12 years of industrial experience with IBM, AT&T, GE, and GAIN, he joined the faculty of Lehigh University, Bethlehem, PA, in 1988, where he is currently a Professor of electrical engineering and the Director of the Compound Semiconductor

Technology Laboratory. In 2002, he helped established the Center for Optical Technologies between Lehigh University and Pennsylvania State University and served as its interim Director. In 2006, he helped establish the IMPACT Center for MEMS/NEMS VLSI between Lehigh University, the University of Illinois, Purdue University, and the Georgia Institute of Technology, and led one of the major tasks. He has been a Nanyang Professor with Nanyang Technological University, Singapore, and an Advisory Professor with Shanghai Jiao Tong University, Shanghai, China. He has been a consultant for the U.S. Government and numerous electronic companies in the areas of RF/microwave devices and integrated circuits. He cofounded GAIN and QED [the latter became a public company (IQEP)]. He has authored or coauthored over 200 technical papers. He holds four U.S. patents.



**Dave I. Forehand** (M'84) received the B.S. and M.S. degrees in chemical engineering from the University of New Mexico, Albuquerque, NM, in 1982 and 1984, respectively.

His research has involved mass spectrometry of aluminum plasma etching, which was conducted at Sandia National Laboratory's Class sub-1 clean-room. From 1989 to 1996, he was with the Defense Systems and Electronics Group (DSEG), Texas Instruments (TI) Incorporated, Dallas, TX, where he was involved with infrared focal plane arrays (IRFPAs). He had sole responsibility for development and manufacturing of all plasma etch and plasma-enhanced chemical vapor deposition (PECVD) processes. His IRFPA achievements include four patents and two trade secrets. He later left TI to join a semiconductor equipment supplier, where he was involved with advanced high-density plasma (HDP) etch systems. He was the Customer Site Lead Engineer responsible for the HDP systems and training of new engineers. He returned to TI in 1998 to become part of a team with the Microcomponents Technology Center to design, develop, and produce the world's first true analog biaxial micromirror for optical switching, which is capable of aiming to  $\sim 1 \mu\text{rad}$ . In April 2001, he joined the RF MEMS Team, Raytheon, to lead the process engineering development activity, during which time he was responsible for transitioning processes for manufacturability and repeatability, as well as developing improvements for increased reliability, which led to a patent. In July 2002, he helped found the MEMtronics Corporation, Plano, TX, where he continues the development and manufacturing of RF MEMS technology for commercial, space, and military applications. He holds three patents with one patent pending for his optical MEMS research.

Mr. Forehand was a recipient of TI's 1995 DSEG Technical Award for Excellence.



**Charles L. Goldsmith** (S'79–M'80–SM'94) received the B.S. and M.S. degrees in electrical engineering from the University of Arizona, Tucson, in 1980 and 1982, respectively, and the Ph.D. degree from the University of Texas at Arlington, in 1995.

Since 1982, he has been involved in the design and development of microwave and millimeter-wave circuits and subsystems. He has been with M/A COM and Texas Instruments Incorporated, and was an Engineering Fellow with the Raytheon Company. He formed the MEMtronics Corporation, Plano, TX, in 2001, where he currently pursues business opportunities for RF MEMS in the commercial and defense markets. Since 1993, he has developed RF MEMS devices and circuits and is the inventor of the capacitive membrane RF MEMS switch. He has spent the last decade dedicated to the development and application of this technology. These activities include the innovation of switches, phase shifters, and tunable antennas for radar and satcom applications, as well as variable capacitors and tunable filters for microwave receiver front ends. He has authored or coauthored over 45 publications on microwave circuits, photonics, and RF MEMS. He is the holder or co-holder of nine patents with three pending in related fields. He was the Guest Editor for three Special Issues on RF Applications of MEMS Technology for the *International Journal of RF and Microwave Computer-Aided Engineering* (Wiley: 1999, 2001, and 2004).

Dr. Goldsmith is a member of the IEEE Microwave Theory and Techniques Society (IEEE MTT-S) and the IEEE Electron Devices Society. He is a member of Tau Beta Pi. He served as chairman and vice-chairman of the IEEE Lasers and Electro-Optics Society (LEOS) Dallas Chapter and currently serves on the IEEE MTT-S Technical Coordinating Committee (TCC-21) on RF MEMS.